Dalton Transactions

Dynamic Article Links

Cite this: *Dalton Trans.*, 2011, **40**, 12801

www.rsc.org/dalton

PAPER

Tin/polypyrrole composite anode using sodium carboxymethyl cellulose binder for lithium-ion batteries

Shu-Lei Chou,*[a,b] Xuan-Wen Gao,[a] Jia-Zhao Wang,*[a,b] David Wexler,[c] Zhao-Xiang Wang,[d] Li-Quan Chen[d] and Hua-Kun Liu[a,b]

Received 10th March 2011, Accepted 20th April 2011
DOI: 10.1039/c1dt10396b

A tin nanoparticle/polypyrrole (nano-Sn/PPy) composite was prepared by chemically reducing and coating Sn nanoparticles onto the PPy surface. The composite shows a much higher surface area than the pure nano-Sn reference sample, due to the porous higher surface area of PPy and the much smaller size of Sn in the nano-Sn/PPy composite than in the pure tin nanoparticle sample. Poly(vinylidene fluoride) (PVDF) and sodium carboxymethyl cellulose (CMC) were also used as binders, and the electrochemical performance was investigated. The electrochemical results show that both the capacity retention and the rate capability are in the same order of nano-Sn/PPy-CMC > nano-Sn/PPy-PVDF > nano-Sn-CMC > nano-Sn-PVDF. Scanning electronic microscopy (SEM) and electrochemical impedance spectroscopy (EIS) results show that CMC can prevent the formation of cracks in electrodes caused by the big volume changes during the charge–discharge process, and the PPy in the composite can provide a conducting matrix and alleviate the agglomeration of Sn nanoparticles. The present results indicate that the nano-Sn/PPy composite could be suitable for the next generation of anode materials with relatively good capacity retention and rate capability.

Introduction

Rechargeable lithium-ion batteries (LIBs) have successfully dominated the commercial power supply market for advanced portable electronics.[1] However, it is still a challenge to develop large cells with high energy density, long cycle life, excellent rate capability, low cost and environmental compatibility for electric vehicles (EVs) and hybrid electric vehicles (HEVs).[2] To meet these requirements, substantial efforts have been made to develop new electrode materials and to design new structures for existing electrode materials.[3–5]

As an anode material for LIBs, metallic tin (Sn) has attracted tremendous interest, owing to its high theoretical capacity of about 990 mA h g^{-1}, as in $Li_{4.4}Sn$, which is significantly higher than that of the currently used graphitic carbon (372 mA h g^{-1} for LiC_6).[6–8] Furthermore, a significant advantage of metallic tin over graphite is that it does not encounter solvent intercalation, which causes irreversible charge loss.[9] Unfortunately, metallic Sn suffers from huge volumetric changes during Li-insertion/extraction cycling, which leads to rapid pulverization and poor cyclability of the materials.[10] Generally, capacity retention can be improved *via* either coating/mixing with conductive/nonconductive materials that can buffer the volume change or by using a new binder.[11,12] For example, Dahn and co-workers reported that composite electrodes with the composition Sn–Fe–C or Sn–Mn–C showed improved cycling performance in lithium cells.[13–15] In 2005, Sony released a new LIB called Nexelion, which used Sn–Co–C composite as its anode material.[16] This further accelerated the interest in lithium alloy electrodes. However, the rate capability of this type of material still needs to be improved.

Recently, the conducting polymer polypyrrole (PPy) has been studied as an additive to improve the performance of cathode and anode materials in LIBs.[17–21] In our previous study,[22] an SnO_2-based PPy composite showed improved capacity and cycle life compared with pure SnO_2, since the conductive PPy in the composite could effectively buffer the great volume changes during the cycling process. At the same time, PPy acts as an efficient host matrix to prevent cracking and pulverization of the SnO_2 electrode due to phase transitions, thus improving the cycling stability of the electrode. Recently, Choi's group reported[23] that Sn-PPy hybrid films have been prepared using the electrodeposition method and tested as anode materials for LIBs. Their tin-PPy hybrid electrode showed a capacity retention of 47%, which is a remarkably enhanced performance compared to a pure tin electrode. However, it is well known that thin film materials can only be used for the production of small batteries and are not suitable for large batteries for EV/HEV applications.

[a]*Institute for Superconducting and Electronic Materials, University of Wollongong, Wollongong, NSW, 2522, Australia*
[b]*ARC Centre of Excellence for Electromaterials Science, University of Wollongong, Wollongong, NSW, 2522, Australia. E-mail: shulei@uow.edu.au, jiazhao@uow.edu.au; Fax: +61 2-4221-5731; Tel: +61 2-4298-1405*
[c]*Faculty of Engineering, University of Wollongong, Wollongong, NSW, 2522, Australia*
[d]*Laboratory for Solid State Ionics, Institute of Physics, Chinese Academy of Sciences, Beijing, 100080, China*

Here, nanosize Sn-PPy composite powder was prepared using a simple chemical method that involved reducing and coating Sn nanoparticles onto the PPy surface.

Material and methods

Materials synthesis

Polypyrrole (PPy) was prepared by the oxidative chemical polymerization method. First, liquid pyrrole monomers and sodium *p*-toluenesulfonate (PTSNa) as a doping agent were dispersed in water. A solution of $FeCl_3$ in water was gradually added into the mixture. The solution was then magnetically stirred for 6 h to complete the polymerization reaction. The resultant black solid product was separated by filtration, washed with acetone and dried in vacuum at 60 °C.

The Sn nanoparticle/PPy (nano-Sn/PPy) composite was prepared as follows: as-prepared polypyrrole powders (150 mg) were added to a 20 ml solution of $SnCl_2{\cdot}2H_2O$ (500 mg) and poly(vinyl pyrrolidone) (PVP) (3 g), and then an aqueous $NaBH_4$ (50 mg) solution (H_2O, 80 ml) was added under an argon atmosphere at room temperature. The reaction was allowed to proceed for 2 h. The final products were then filtered, washed with de-ionized water and dried at 70 °C in a vacuum over for 12 h. Pure nano-Sn was also prepared by a procedure similar to that for the composite, but without adding PPy.

Materials characterization

The morphology and microstructure of the nano-Sn/PPy composite were characterized by X-ray diffraction (XRD; Philips PW1730), the Brunauer–Emmett–Teller technique (BET; Quanta Chrome Nova 1000), scanning electron microscopy (SEM; JEOL FESEM-7500, 30 kV, equipped for energy dispersive X-ray (EDX) spectroscopy), transmission electron microscopy (TEM; JEOL 2011, 200 kV) and Raman spectroscopy. Raman spectra were recorded using a JOBIN Yvon Horiba Raman Spectrometer model HR800, employing a 10 mW helium/neon laser at 632.8 nm, which was filtered by a neutral density filter to reduce the laser intensity, and a charge-coupled detector (CCD).

Electrochemical characterizations

To test the electrochemical performance, the as-prepared nano-Sn/PPy composite or the nano-Sn were mixed at a ratio of 70 wt% active materials (nano-Sn or nano-Sn/PPy) with 20 wt% carbon black and 10 wt% binder, sodium carboxymethyl cellulose (CMC) or poly(vinylidene fluoride) (PVDF). The slurry made by using water or *N*-methyl-2-pyrrolidone (NMP) as the solvent for CMC and PVDF, respectively, was uniformly pasted onto pieces of Cu foil with an area of 1 cm^2. Such prepared electrode sheets were dried at 90 °C in a vacuum oven for 12 h. Then, the electrodes were compressed before making the cells. The electrochemical cells (CR 2032 coin-type cells) that were prepared for testing included the as-prepared nano-Sn/PPy composite or the nano-Sn on copper foil as the working electrode, Li foil as the counter and reference electrode, a porous polypropylene film as the separator, and 1 M $LiPF_6$ (battery grade 99.99%, Aldrich) in a 1 : 2 (v/v) mixture of ethylene carbonate (EC, anhydrous 99%, Sigma-Aldrich) and diethyl carbonate (DEC, anhydrous 99+%, Sigma-Aldrich) as the electrolyte. The cells were assembled in an Ar-filled glove box. The cells were cycled at a current density of 0.1 C (1 C = 990 mA g^{-1}) for the first 5 cycles and then cycled at different current densities for the following cycles between 0.01 and 1.5 V using a computer-controlled charger system manufactured by Land Battery Testers. Electrochemical impedance spectroscopy (EIS) was conducted using a Biologic VMP-3 electrochemical workstation. The specific capacity is based on the weight of the nano-Sn or nano-Sn/PPy composite material. The typical electrode weight was approximately 3 mg cm^{-2}.

Results and discussion

Structure and morphologies

The tin nanoparticle/polypyrrole (nano-Sn/PPy) composite was prepared by chemically reducing and coating nanosized Sn onto the PPy surface. X-Ray diffraction (XRD) patterns and Raman spectra for the nano-Sn, pristine PPy and nano-Sn/PPy composite are shown in Fig. 1. All the diffraction peaks in the XRD patterns of the nano-Sn and nano-Sn/Ppy composite (Fig. 1(a)) can be indexed to a tetragonal Sn phase with space group *I41/amd* (JCPDS no. 04-0673). No peaks of any other phases were detected. The peaks of the composite are much broader than those of the pure nano-Sn, indicating the much smaller crystal size of Sn in the Sn/PPy composite. The crystal size of the nano-Sn and nano-Sn/PPy composite calculated *via* the Debye–Scherrer equation from the (200) peak was 107.0 and 17.6 nm, respectively. The crystal size of the nano-Sn in the PPy composite is much smaller than that in the pure nano-Sn. The high background of the Sn/PPy composite at around 25 to 35° is due to the presence of PPy. Raman spectra, as shown in Fig. 1(b), confirmed the presence of crystallized Sn with a band located at 206 cm^{-1} for both nano-Sn and Sn/PPy composite samples. Other peaks from 800 to 1700 cm^{-1} can be assigned to pure PPy.[24] The specific surface areas of the as-prepared products were measured

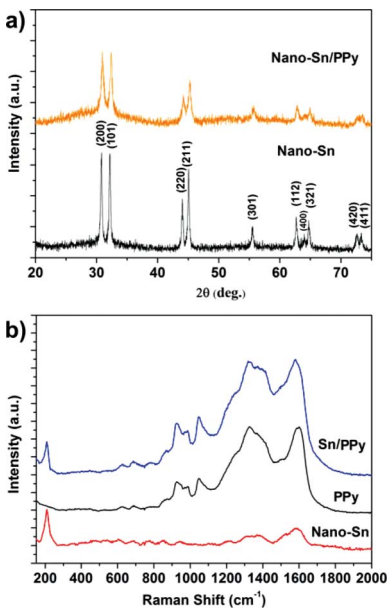

Fig. 1 XRD patterns (a) and Raman spectra (b) of nano-Sn, PPy and the Sn/PPy composite.

by the 15-point Brunauer–Emmett–Teller (BET) N_2 adsorption method. The specific surface area of the nano-Sn and nano-Sn/PPy composite was 6.0 and 25.0 m^2 g^{-1}, respectively. The composite shows a much higher surface area than the pure nano-Sn sample. This probably is due to the porous high surface area of PPy and the much smaller crystal size of Sn in the nano-Sn/PPy composite sample. The weight content of Sn in the composite was quantitatively analyzed by chemical analysis. The composite was dispersed in dilute HCl, in which the Sn was dissolved. Then, the dispersion was filtered, washed with de-ionized water and finally dried in a vacuum oven at 60 °C for 12 h. The filtered material only contained PPy. Therefore, by weighing the dried material, the content of PPy in the as-prepared composite was determined to be approximately 25%.

Typical scanning electron microscope (SEM) images of the PPy, nano-Sn and nano-Sn/PPy composite are shown in Fig. 2. Fig. 2(a) shows the typical morphology of PPy, with an average particle size of around 500 nm. Fig. 2(b) shows Sn nanoparticles that are agglomerated together. The average particle size is around 30–50 nm. Fig. 2(c) displays an SEM image of the nano-Sn/PPy composite. The morphology of the composite is similar to that of PPy. The difference is that the nano-Sn/PPy composite shows a much rougher surface with small particles attached to the surface of the PPy. The small particles could be Sn nanoparticles.

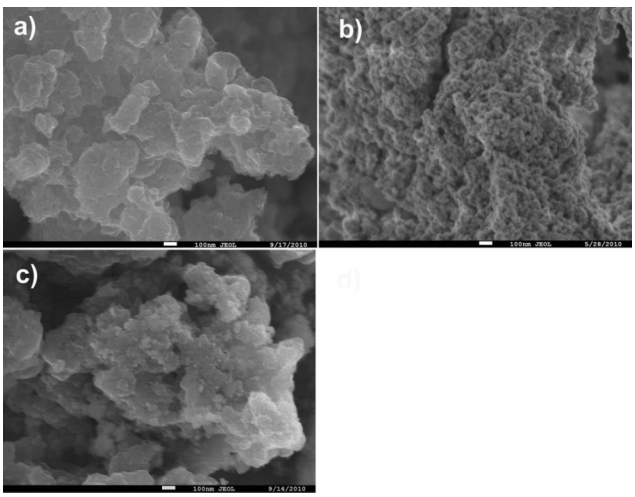

Fig. 2 SEM images of PPy (a), nano-Sn (b) and the nano-Sn/PPy composite (c). The scale bars are all 100 nm.

In order to further confirm the presence of Sn, energy dispersive X-ray (EDX) mapping was used to observe the distribution of Sn. The results are shown in Fig. 3. The color points are due to the presence of the element. The elements N and C are present due to the presence of PPy. It can be seen that the Sn is homogenously distributed on the surface of the PPy particles.

Transmission electron microscopy (TEM) was used to further confirm the presence of Sn nanoparticles in the composite. The Sn/PPy composite was ground using a mortar, suspended in ethanol *via* ultrasonication and loaded onto a holey carbon support film on a copper grid for TEM observations. Typical TEM images are shown in Fig. 4. Fig. 4(a) shows a low magnification TEM image. There is different contrast because the particle is composed of two types of material. The darker spots are Sn nanoparticles, while the gray background is PPy particles. Fig. 4(b)

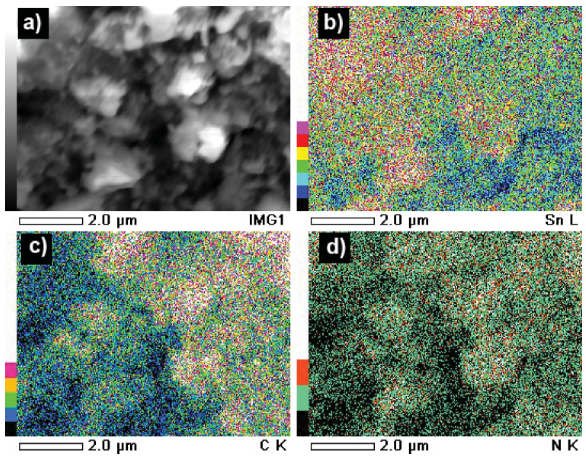

Fig. 3 SEM image (a), and EDX mapping of the nano-Sn/PPy composite for the elements Sn (b), C (c) and N (d).

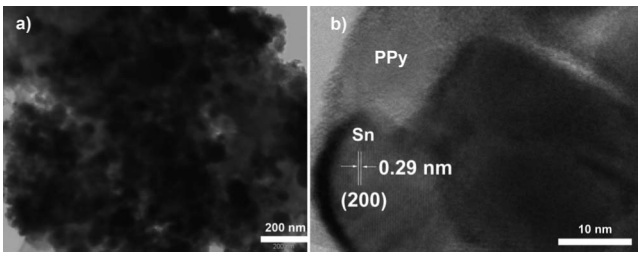

Fig. 4 Typical TEM (a) and HRTEM (b) images of the nano-Sn/PPy composite.

contains a high resolution TEM (HRTEM) image of the edge of a particle. Lattice fringes can be observed for a Sn nanoparticle, indicating the crystalline structure of the Sn. The particle size is around 10 nm. The amorphous PPy can also be seen in the background.

Electrochemical characterization

Fig. 5 shows the charge–discharge curves for the nano-Sn and nano-Sn/PPy composite electrodes using CMC and PVDF as the binder, respectively. The pure nano-Sn electrode with PVDF

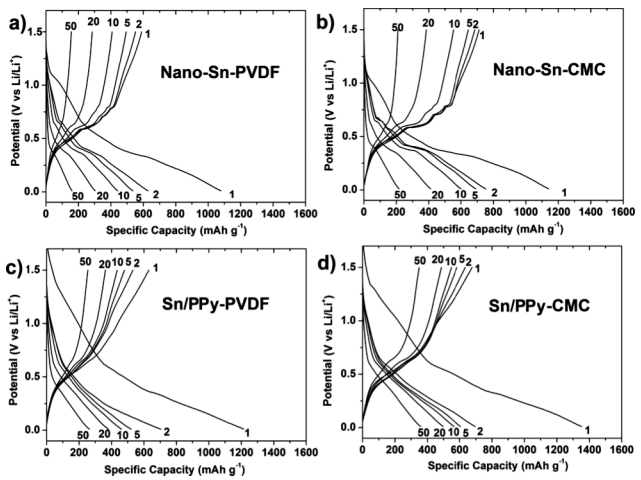

Fig. 5 Charge–discharge curves of nano-Sn (a, b) and nano-Sn/PPy composite (c, d) using PVDF (a, c) and CMC (b, d) as the binder, respectively.

the as binder (Fig. 5(a)) shows multistep charge and discharge curves, which are similar to those in previous reports.[25] The nano-Sn electrode using CMC as the binder shows similar curves, but with a much higher capacity and better retention. The initial discharge capacity of the nano-Sn using PVDF and CMC as the binder was 1079 and 1142 mA h g^{-1}, respectively. The second cycle discharge capacity was 630 and 752 mA h g^{-1}, respectively. The reversible capacity of the nano-Sn electrode using PVDF and CMC as the binder was 58.4 and 65.8% of initial capacity, respectively. A previous report showed that CMC can be used as a binder to enhance the cycling stability of SnO_2-based materials.[12] The present results show the great enhancement of electrochemical performance, including both initial capacity and reversible capacity, when CMC is used as the binder for Sn nanoparticles.

Fig. 5(c) and (d) display the charge and discharge curves of the nano-Sn/PPy composite electrode using PVDF and CMC as the binder, respectively. The charge and discharge curves show sloping curves with no obvious multiple plateaus, which is different from that seen for the nano-Sn electrode. The initial discharge capacities of the nano-Sn/PPy composite electrodes using PVDF and CMC as the binder were 1215 and 1394 mA h g^{-1}, respectively, which is ~200 mA h g^{-1} higher than for the nano-Sn electrode. This additional ~200 mA h g^{-1} capacity mainly comes from voltages higher than 0.6 V, in which range the capacity is mainly due to the formation of the solid electrolyte interphase (SEI) layer, because the capacity contribution from pure PPy is negligible.[26] Since the Sn/PPy composite features a much higher surface area, the formation of the SEI layer in the composite electrode is much more intense than in the pure nano-Sn electrode. Therefore, the initial discharge capacity of the Sn/PPy composite electrode is much higher than that of the nano-Sn electrode. The second cycle discharge capacities of Sn/PPy composite electrodes using PVDF and CMC as the binder are both ~700 mA h g^{-1}. The theoretical specific capacity of the Sn/PPy composite is 742 mA h g^{-1} based on 75% Sn in the composite. The second discharge capacity is close to the theoretical capacity. This value is higher than that for the nano-Sn electrode using PVDF as the binder, but lower than that for the nano-Sn electrode using CMC as the binder. That is to say, the CMC binder and the Sn/PPy composite can both improve the reversible capacity of Sn-based materials.

dQ/dV plots corresponding to the charge and discharge curves in Fig. 5 are shown in Fig. 6. The dQ/dV curves for the nano-Sn electrode using PVDF as the binder (Fig. 6(a)) are in good agreement with a previous report.[27] During the initial complete scan, the first peak at around 1.05 V *vs.* Li/Li^+ is probably due to irreversible reactions between lithium and surface species of the Sn nanoparticles. The small peak at 0.5–0.6 V is related to SEI layer formation. The sharp peak at 0.33 V is due to the phase transition of Li_xSn. During the second discharge, two peaks are observed at 0.65 and 0.4 V, in contrast to the first discharge. Four sharp peaks are observed in the charge process, indicating the multistep nature of the phase change. The nano-Sn electrode using CMC as the binder shows similar dQ/dV plots in terms of peak position, indicating that the electrochemical reactions for both binders are similar, while the intensities of the peaks are higher than those for the PVDF electrode, indicating the better cycling stability.

Fig. 6(c) and (d) present the dQ/dV plots of the Sn/PPy composite electrodes using PVDF and CMC as the binder,

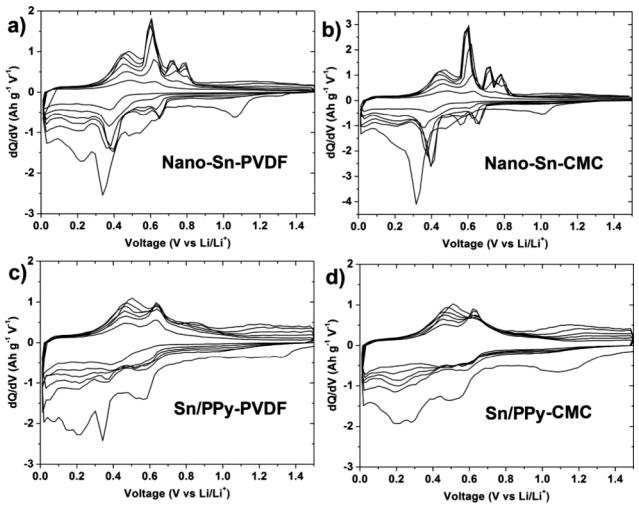

Fig. 6 dQ/dV plots of Sn (a, b) and the nano-Sn/PPy composite (c, d) using PVDF (a, c) and CMC (b, d) as the binder, respectively.

respectively. It should be noted that the differential plots for the composite show suppression of the sharp peaks of pure nano-Sn. There are only two peaks that can be clearly observed during the charge process. Furthermore, the peak positions are also shifted due to the change in the phase transition voltages. A similar behavior was reported for the Sn–C composite, with suppressed phase transitions or changes in the phase transition voltages.[26] This may be because the PPy composite may be able to influence the overall phase-change rate. The peak intensities of the nano-Sn/PPy composite using CMC as the binder show a better stability than those of the electrode using PVDF as the binder, indicating the better capacity retention of the nano-Sn/PPy composite electrode using CMC as the binder.

The cycling stabilities of the nano-Sn and the nano-Sn/PPy composite using CMC as the binder are shown in Fig. 7. The discharge capacity of the nano-Sn/PPy composite using CMC and PVDF as the binder at the 50th cycle is ~400 and ~250 mA h g^{-1}, respectively, while that of the nano-Sn using CMC and PVDF as the binder at the 50th cycle is only ~210 and ~150 mA h g^{-1}, respectively. The capacity retention is in the order nano-Sn/PPy-CMC > nano-Sn/PPy-PVDF > nano-Sn-CMC > nano-Sn-PVDF. The coulombic efficiency for nano-Sn/PPy and nano-Sn using CMC as the binder is around 98.7 and 95.6%, respectively,

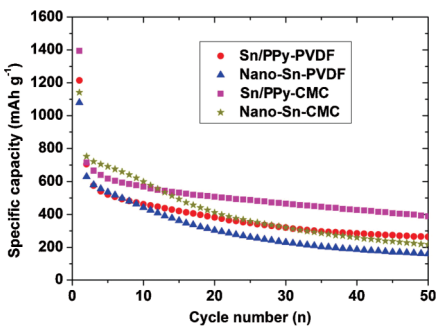

Fig. 7 Cycle life of nano-Sn and nano-Sn/PPy composite electrodes using CMC and PVDF as the binder, respectively. The cycles are all between 0.01 and 2.0 V *vs.* Li/Li^+ at 25 °C, with a current density of 0.1 C for the first cycle and 0.2 C for the following cycles.

indicating the better electrochemical reversibility of the nano-Sn/PPy composite electrode. The nano-Sn/Ppy composite using CMC as the binder shows the best capacity retention, which is comparable to values reported for nano-Sn/PPy composite thin film (400 mA h g^{-1} after 50 cycles).[23] However, the capacity retention is still not as good as with Sn/carbon composites, such as the Sn/carbon hollow sphere composite (550 mA h g^{-1} after 100 cycles;[11] 500 mA h g^{-1} after 200 cycles[8]) or the Sn/amorphous carbon composite (700 mA h g^{-1} after 50 cycles[27]). Using both PPy composite as the active material and CMC as the binder can improve the capacity retention of nano-Sn. Here, we need to point out that the smaller size of the Sn nanoparticles in the composite may also contribute to the enhanced capacity retention. Therefore, further enhancements in capacity retention are expected with proper optimization of the composition and morphology, and the addition of a protective coating layer on the surface of tin nanoparticles.[27–29]

Changing the charge–discharge rate was also used for characterizing the stability of the nano-Sn and nano-Sn/PPy composite electrodes using CMC and PVDF as the binder, as shown in Fig. 8(a). The nano-Sn/PPy composite electrode using CMC as the binder showed the highest specific capacity of 220 mA h g^{-1} at a current density of 4 C. There is less than a 10% capacity loss for the nano-Sn/Ppy composite electrode using CMC as the binder after changing the current density from 0.1 to 4 C and back to 0.1 C in 35 cycles, showing the relatively good cycling stability. Rate capability plots are presented in Fig. 8(b) to show the rate capability of the nano-Sn and nano-Sn composite using PVDF and CMC as the binder. It can be seen that the rate performance follows the order nano-Sn/PPy-CMC > nano-Sn/PPy-PVDF > nano-Sn-CMC > nano-Sn-PVDF, which is the same order as for capacity retention.

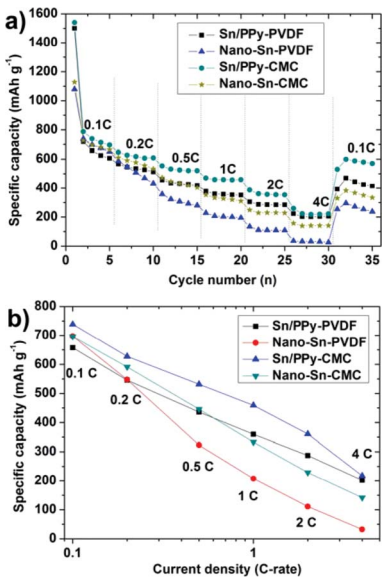

Fig. 8 (a) Specific capacities of nano-Sn and nano-Sn/PPy composite using CMC and PVDF as the binder at different current densities. (b) Rate capabilities of nano-Sn and nano-Sn/PPy composite using CMC and PVDF as the binder with changing current density from 0.1 C to 4 C and back to 0.1 C (C = 990 mA h g^{-1}) between 0.01 and 1.5 V *vs.* Li/Li^+ at 25 °C.

In order to investigate the reason for the enhanced capacity retention by using the CMC binder and the PPy composite, the electrodes were washed and dried after cycling, and the changes in morphology were examined by SEM. SEM images of the surface of the electrodes before and after cycling are shown in Fig. 9. The left-hand side SEM images show the electrode surfaces before cycling, while the right-hand side shows the surfaces after 50 cycles. The electrodes before cycling show a similar smooth surface, while after cycling, the electrode morphology shows big differences. Fig. 9(b) is an SEM image of the nano-Sn electrode using PVDF as the binder after 50 cycles. There are large agglomerations of particles of 50 μm in size and clearly visible cracks. The poor morphology retention gives poor capacity retention. From Fig. 9(d), it can be seen that using CMC as the binder can protect the electrode from cracking but cannot prevent the nano-Sn from agglomerating. This is also the reason why using CMC can temporarily improve the capacity retention, but eventually the capacity falls. Fig. 9(f) is an SEM image of the nano-Sn/PPy composite using PVDF as the binder. The agglomeration of Sn particles is significantly relieved compared to the nano-Sn, but there are still clearly visible cracks in the electrode. The PPy could be acting as a conductive matrix, while preventing the agglomeration of Sn nanoparticles, and buffering the volume change during lithium alloying and de-alloying. It is worth pointing out that the much smaller size of the Sn nanoparticles in the nano-Sn/PPy composite than in pure nano-Sn could also alleviate the volume change. However, the

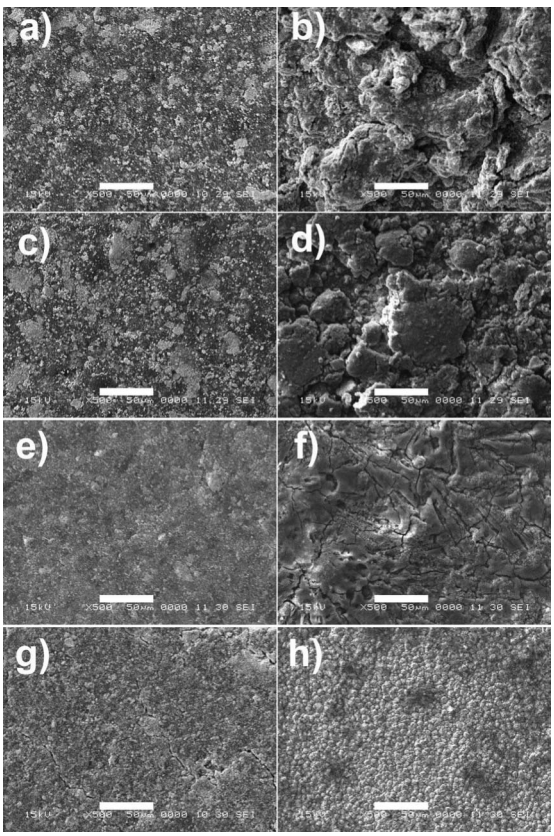

Fig. 9 SEM images of the electrode surface of nano-Sn (a–d) and nano-Sn/PPy composite (e–h) using PVDF (a, b, e, f) and CMC (c, d, g, h) as the binder before (a, c, e, g) and after (b, d, f, h) 50 cycles. The scale bars are all 50 μm.

cracks in the electrode will affect the electrochemical performance. The electrode surface of the nano-Sn/PPy composite using CMC as the binder is much smoother in Fig. 9(h). There are no clear cracks, nor can large-scale agglomeration be observed on the surface. The average particle size is 5 μm, which is about 10% of the particle size in the nano-Sn electrode using CMC as the binder. Therefore, CMC can prevent the formation of cracks in electrodes during the charge–discharge process, despite big volume changes, while the PPy in the composite can provide a conducting matrix and alleviate the agglomeration of Sn nanoparticles.

Electrochemical impedance spectroscopy (EIS) was used to further investigate the reasons for the enhanced rate capability and capacity retention of the nano-Sn and nano-Sn/PPy composite using CMC as the binder. Fig. 10(a) shows the Nyquist plots of the different electrodes at a discharge potential of 0.3 V *vs.* Li/Li^+ after charging–discharging for 5 and 50 cycles. All the impedance curves show one compressed semicircle in the medium frequency region, which could be assigned to charge transfer resistance (R_{ct}) and an approximately 45° inclined line in the low-frequency range, which could be considered as Warburg impedance. Composite electrodes show another small semicircle in the high frequency region (Fig. 10(b). This semicircle at higher frequencies is believed to be closely related to the PPy conductivity, as expressed in the electron transfer.[30] The R_{ct} for the composite includes both R_{PPy} (resistance from PPy) and R_2 (resistance from others), which can be calculated using the equivalent circuit shown in the inset of Fig. 10(a). R_{PPy} is 4 and 10 Ω cm^{-2} for the nano-Sn/PPy composite electrode using CMC as the binder before and after cycling, respectively. R_2 is 20 and 50 Ω cm^{-2} for the nano-Sn/PPy composite electrode using CMC as the binder before and after cycling, respectively, while it is 51 and 150 Ω cm^{-2} for the nano-Sn electrode using CMC as the binder before and after cycling, respectively. The total R_{ct} for the nano-Sn/PPy composite electrode before and after cycling is still much lower than that of the nano-Sn electrode, indicating the enhanced electron transfer due to the good conductivity of PPy. After 5 and 50 cycles, the R_{ct} for both the nano-Sn and the nano-Sn/PPy composite increases, indicating increasing resistance. This is related to the change in the morphology of the electrodes. The R_{ct} of the nano-Sn/PPy composite electrode only increases by around 2.5 times, while that of the nano-Sn increases by around 3 times, indicating good capacity retention.

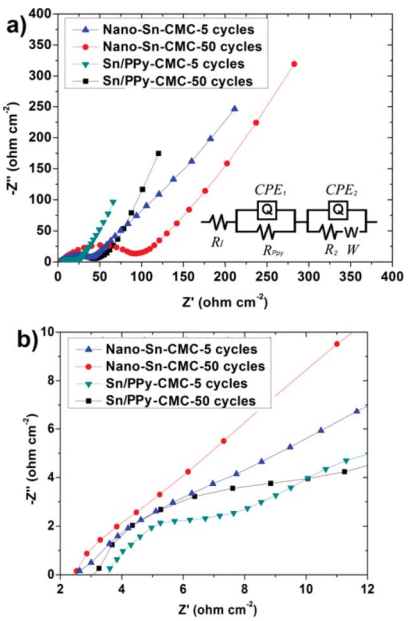

Fig. 10 (a) Nyquist plots of nano-Sn and Sn/PPy composite using CMC as the binder after cycling over 5 and 50 cycles at a discharge potential of 0.3 V *vs.* Li/Li^+ at 25 °C at frequencies from 100 kHz to 20 mHz. (b) Enlargement of (a) in the high frequency range. The inset in (a) is the equivalent circuit used.

Conclusions

A nano-Sn/PPy composite was prepared by chemically reducing and coating Sn nanoparticles onto the PPy surface. The composite sample showed a much higher surface area than the pure nano-Sn sample due to the higher surface area of the PPy and the much smaller crystal size of Sn in the nano-Sn/PPy composite than in the pure Sn nanoparticle sample. The electrochemical results show that both the capacity retention and the rate capability are in the same order: nano-Sn/PPy-CMC > nano-Sn/PPy-PVDF > nano-Sn-CMC > nano-Sn-PVDF. The results show that CMC can prevent the formation of cracks in electrodes during the charge–discharge process, despite the big volume changes. The R_{ct} for the nano-Sn/PPy composite electrode before and after cycling is still much lower than that of the nano-Sn electrode, indicating enhanced electron transfer due to the good conductivity of PPy. The PPy could be acting as a conductive matrix, while preventing the agglomeration of Sn nanoparticles and buffering the volume change during lithium alloying and de-alloying. In addition, the size of the Sn nanoparticles in the nano-Sn/PPy composite is much smaller than in pure nano-Sn. This indicates that the PPy can be a great dispersion agent to prepare small Sn nanoparticles. The present results indicate that the nano-Sn/PPy composite could be suitable for the next generation of anode materials with relatively good capacity retention and rate capability.

Acknowledgements

Financial support was provided by the Australian Research Council (ARC) through a Discovery project (DP0987805) and ARC Centre of Excellence funding (CE0561616). Additional funding from the Department of Innovation, Industry, Science and Research, Australia *via* an International Linkage Project (CH 090014) is also gratefully acknowledged. The authors also want to thank Dr T. Silver for critically reading the manuscript.

References

1 M. S. Whittingham, *Chem. Rev.*, 2004, **104**, 4271.
2 M. Armand and J. M. Tarascon, *Nature*, 2008, **451**, 652.
3 (*a*) P. G. Bruce, B. Scrosati and J. M. Tarascon, *Angew. Chem., Int. Ed.*, 2008, **47**, 2930; (*b*) M. S. Whittingham, *Dalton Trans.*, 2008, 5424.
4 P. Gomez-Romero, *Adv. Mater.*, 2001, **13**, 163.
5 (*a*) H. Li, Z. X. Wang, L. Q. Chen and X. J. Huang, *Adv. Mater.*, 2009, **21**, 4593; (*b*) Y. Xie and C. Z. Wu, *Dalton Trans.*, 2007, 5235; (*c*) T. Zhang, J. Gao, L. J. Fu, L. C. Yang, Y. P. Wu and H. Q. Wu, *J. Mater. Chem.*, 2007, **17**, 1321.
6 J. Yang, M. Winter and J. O. Besenhard, *Solid State Ionics*, 1996, **90**, 281.
7 K. T. Lee, Y. S. Jung and S. M. Oh, *J. Am. Chem. Soc.*, 2003, **125**, 5652.
8 G. Derrien, J. Hassoun, S. Panero and B. Scrosati, *Adv. Mater.*, 2007, **19**, 2336.

9 M. Winter, J. O. Besenhard, M. E. Spahr and P. Novak, *Adv. Mater.*, 1998, **10**, 725.
10 M. Winter and J. O. Besenhard, *Electrochim. Acta*, 1999, **45**, 31.
11 W. M. Zhang, J. S. Hu, Y. G. Guo, S. F. Zheng, L. S. Zhong, W. G. Song and L. J. Wan, *Adv. Mater.*, 2008, **20**, 1160.
12 S. L. Chou, J. Z. Wang, C. Zhong, M. M. Rahman, H. K. Liu and S. X. Dou, *Electrochim. Acta*, 2009, **54**, 7519.
13 O. Mao, R. A. Dunlap and J. R. Dahn, *J. Electrochem. Soc.*, 1999, **146**, 405.
14 O. Mao and J. R. Dahn, *J. Electrochem. Soc.*, 1999, **146**, 423.
15 L. Y. Beaulieu and J. R. Dahn, *J. Electrochem. Soc.*, 2000, **147**, 3237.
16 http://www.sony.net/SonyInfo/News/Press/200502/05-006E/.
17 A. Du Pasquier, F. Orsini, A. S. Gozdz and J. M. Tarascon, *J. Power Sources*, 1999, **81–82**, 607.
18 B. Veeraraghavan, J. Paul, B. Hala and B. Popvo, *J. Power Sources*, 2002, **109**, 377.
19 G. X. Wang, L. Yang, Y. Chen, J. Z. Wang, S. Bewlay and H. K. Liu, *Electrochim. Acta*, 2005, **50**, 4649.
20 J. Wang, J. Chen, K. Konstantinov, L. Zhao, S. H. Ng, G. X. Wang, Z. P. Guo and H. K. Liu, *Electrochim. Acta*, 2006, **51**, 4634.
21 K. S. Park, S. B. Schougaard and J. B. Goodenough, *Adv. Mater.*, 2007, **19**, 848.
22 L. Yuan, J. Wang, S. Y. Chew, J. Chen, Z. P. Guo, L. Zhao, K. Konstantinov and H. K. Liu, *J. Power Sources*, 2007, **174**, 1183.
23 Y. Jung, N. Singh and K. S. Choi, *Angew. Chem., Int. Ed.*, 2009, **48**, 8331.
24 Y. Furukawa, S. Tazawa, Y. Fujii and I. Harada, *Synth. Met.*, 1988, **24**, 329.
25 J. Yang, Y. Takeda, N. Imanishi and O. Yamamoto, *J. Electrochem. Soc.*, 1999, **146**, 4009.
26 P. Novak, K. Muller, K. S. V. Santhanam and O. Haas, *Chem. Rev.*, 1997, **97**, 207.
27 M. Noh, Y. Kwon, H. Lee, J. Cho, Y. Kim and M. G. Kim, *Chem. Mater.*, 2005, **17**, 1926.
28 H. Lee and J. Cho, *Nano Lett.*, 2007, **7**, 2638.
29 Y. Kwon, H. Kim, S. G. Doo and J. Cho, *Chem. Mater.*, 2007, **19**, 982.
30 T. Osaka, K. Naoi, S. Ogano and S. Nakamura, *J. Electrochem. Soc.*, 1987, **134**, 2096.